

Magnetic Nanoparticles Based on DABCO as Catalysts in the Knoevenagel Reaction and Synthesis of Isatin- β -thiosemicarbazones

Nathália K. S. M. Falcão,^a Gilvan P. Pires,^a Paloma G. Abrantes,^a Poliana G. Abrantes,^a João B. M. Resende Filho,^b Claudio G. Lima Junior,^b ^a Ercoles E. S. Teotonio ^{a,c} and Juliana A. Vale ^{*,a}

^aDepartamento de Química, CCEN, Universidade Federal da Paraíba, 58051-900 João Pessoa-PB, Brazil

^bInstituto Federal de Educação, Ciência and Tecnologia da Paraíba, Campus Sousa, Av. Presidente Tancredo Neves, s/n, Jardim Sorrilândia, 58800-970 Sousa-PB, Brazil

^cInstitute of Inorganic Chemistry, Christian-Albrechts-Universität zu Kiel, Max-Eyth-Str. 2, Kiel, D-24118, Germany

This work describes the route to prepare a novel core-shell catalyst based on 1,4-diazabicyclo[2,2,2]octane (DABCO) supported magnetic nanoparticles (MNPs). The morphology and composition of the obtained catalysts were characterized by Fourier-transform infrared (FTIR) spectroscopy, thermogravimetric analysis (TGA), X-ray powder diffraction (XRD), transmission electron microscopy (TEM), quantum design vibrating sample magnetometer (VSM) and scanning electron microscopy (SEM). These nanomaterials presented high performance as a basic catalyst for Knoevenagel condensation between malononitrile and aldehydes, leading to products with excellent yields (84-99%) and short reaction times (5-60 min). Furthermore, it was also efficient in the condensation of isatins with 4-phenylthiosemicarbazide, resulting in isatin- β -thiosemicarbazones with high yields (81-94%) and short times (60-180 min). It is worth mentioning that the catalyst was recovered and reused in these two kinds of reactions after six cycles without significant yield loss.

Keywords: Fe₃O₄ nanoparticles, DABCO, Knoevenagel condensation, isatin- β -thiosemicarbazones

Introduction

In the last decades, magnetic nanoparticles (MNPs) have been the focus of several studies due to their important properties, such as low toxicity, high activity, thermal stability, surface modification capability, easy dispersion,¹⁻⁴ and high stability against organic solvents.⁵ Such characteristics make them suitable to act in several areas, such as biosensors,⁶ drug carriers, magnetic resonance imaging,⁷ besides also standing out as sustainable and promising support in the field of catalysis.⁸⁻¹⁰ The high surface area of nanoparticles ensures the control and high loading of the catalyst, enabling an excellent interaction between the reactants and the catalytic center, as occurs in homogeneous catalysis.¹¹

The use of magnetic nanoparticles as a heterogeneous catalyst has been reported in various organic reactions,

including asymmetric, environmental, acid-base, oxide-reduction, hydrogenation, multicomponent synthesis, and C-C coupling catalysis.¹¹⁻¹⁵ Among the various types of C-C coupling reactions of organic compounds, Knoevenagel condensation stands out as one of the most important,² as it acts as a key step in the synthesis of numerous bioactive molecules.¹⁶ Several catalysts and reaction methods have been reported for Knoevenagel condensation, such as amino acid functionalized silica,¹⁷ γ -Fe₂O₃ encapsulated in hydroxyapatite,¹⁸ functionalized chitosan,¹⁹ metal-organic framework (MOF),²⁰ functionalized polyoxomolybdates,²¹ carbon nanotube based monodisperse nanohybrids.²² However, the synthesis of Knoevenagel compounds takes place with times varying from a few minutes to several hours, depending on the nature of the reactants.

Another reaction that is also becoming prominent is the synthesis of thiosemicarbazones due to the excellent implications in studies involving their derivatives as well as the vast pharmacological applications as antimicrobial,

*e-mail: julianadqf@yahoo.com.br

Editor handled this article: Brenno A. D. Neto

antituberculosis, antitumor, and antiviral.²³ Some works describing alternative methods for synthesizing isatin- β -thiosemicarbazones have been reported in the literature.²⁴⁻²⁷ However, the use of magnetic nanocatalyst for the synthesis of this compound is still unknown.

Herein, we report the preparation of 1,4-diazabicyclo[2,2,2]octane (DABCO) functionalized MNPs and their applications in heterogeneous catalysis to obtain isatin- β -thiosemicarbazones from the reaction between isatins and 4-phenylthiosemicarbazides as well as in the Knoevenagel condensation reaction between aldehydes and malononitrile. In addition, the study of recyclability of the nanocatalyst in both reactions is also reported.

Experimental

Materials

Iron(III) chloride hexahydrate ($\text{FeCl}_3 \cdot 6\text{H}_2\text{O}$, min. 97%), iron(II) chloride tetrahydrate ($\text{FeCl}_2 \cdot 4\text{H}_2\text{O}$, min. $\geq 99\%$), sodium hydroxide (NaOH, min. $\geq 97\%$), hydrochloric acid (HCl, min. 97%), polyvinylpyrrolidone (PVP, average molecular weight 40.000 Da), tetraethoxysilane (TEOS, min. 98%), ammonium hydroxide solution (NH_4OH , 28.0-30.0% NH_3 basis), 3-chloropropyltrimethoxysilane (min. 97%), and 1,4-diazabicyclo[2,2,2]octane (DABCO, min. 97%) were purchased from Sigma-Aldrich (São Paulo, Brazil). Pyridine (min. $\geq 99.0\%$), and acetic anhydride (min. $\geq 99.0\%$) were stored under molecular sieve (3 Å) were purchased from Sigma-Aldrich (São Paulo, Brazil). The solvents ethanol (min. 99.98%), methanol (min. 99.98%), chloroform (min. 99.9%), hexane (min. 99%), ethyl ether (min. 99%) and tetrahydrofuran (min. 99.8%) were obtained from Tedia (Ohio, USA). Aldehydes, ketones and malononitrile were purchased from Sigma-Aldrich (São Paulo, Brazil).

Apparatus

Fourier-transform infrared (FTIR) spectra were recorded on an IR Tracer-100 FT-IR spectrophotometer (Shimadzu, Osaka, Japan) using the dispersion technique in KBr, in a range spectral range from 400 to 4000 cm^{-1} . Thermogravimetric analyses were performed on a DTG-60H model (Shimadzu, Osaka, Japan) at a heating rate of 10 $^\circ\text{C min}^{-1}$ flux of nitrogen of 50 mL min^{-1} and temperature range from 25 to 900 $^\circ\text{C}$. Surface morphology was studied by scanning electron microscopy (SEM) Quanta 450 FEG (FEI company, Hillsboro, USA), 25 kV, and transmission electron microscopy (TEM) using model JEM-1200 (JEOL Ltd., Tokyo, Japan) operating at

120 kV. Measurements of carbon, nitrogen, and hydrogen percentages were performed by a PerkinElmer model 2400 elemental microanalysis (Devon, England). X-ray diffraction (XRD) patterns of the materials were recorded with a Lab-X XRD-6000 diffractometer (Shimadzu, Osaka, Japan), using $\text{Cu K}\alpha$ radiation ($\lambda = 0.154056 \text{ nm}$). Measurements of magnetization curves at room temperature were performed by using a Quantum Design vibrating sample magnetometer (VSM) from VersaLab (Budapest, Hungary) under a test field range of -10.000 to 10.000 Oe . The products of the reactions were characterized by hydrogen and carbon-13 nuclear magnetic resonance spectra recorded on a VARIAN Mercury Spectra AC 20 spectrometer 50, 75, 200, 300 and 400 MHz (California, USA).

Catalyst preparation

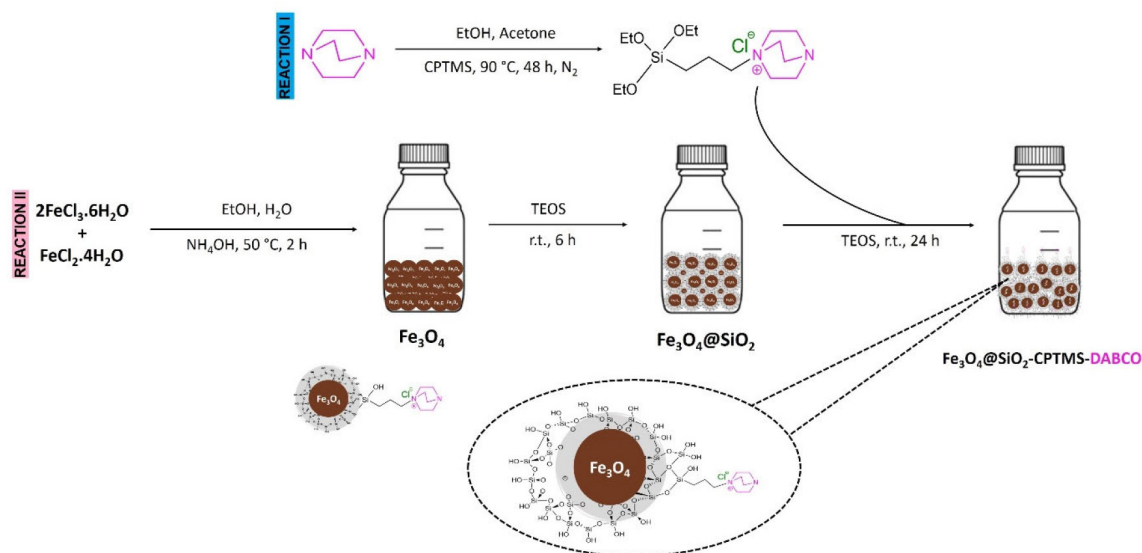
The $\text{Fe}_3\text{O}_4 @ \text{SiO}_2$ -CPTMS-DABCO catalyst was developed by means of a proposed synthesis comprising two reactions occurring concomitantly, as described in Scheme 1.

Reaction I: the synthesis of CPTMS-DABCO was performed according to Arenas *et al.*^{28,29} 0.224 g (2 mmol) of DABCO was dissolved in 4 mL of ethanol/acetone solution (1:1), and then 414 μL (2 mmol) of 3-chloropropyltrimethoxysilane (CPTMS) was added to the reaction medium. The system was kept at reflux under magnetic stirring and inert atmosphere for 48 h. The product formed is colorless and gelatinous in appearance.

Reaction II: the synthesis of $\text{Fe}_3\text{O}_4 @ \text{SiO}_2$ nanoparticles were performed in a closed tube (duran/Schott), as follows: 0.34 g of $\text{FeCl}_3 \cdot 6\text{H}_2\text{O}$ (1.2 mmol) and 0.15 g of $\text{FeCl}_2 \cdot 4\text{H}_2\text{O}$ (0.7 mmol) and 50 mL of ethanol/distilled water solution (4:1). The system was heated at 50 $^\circ\text{C}$, and then 0.8 mL of a NH_4OH solution was added dropwise and under vigorous stirring. The reaction was kept under heating and magnetic stirring for 2 h. After this period, the system was brought to room temperature, and 0.5 mL of tetraethoxysilane (TEOS) was added. The reaction proceeded under magnetic stirring and at room temperature for 6 h. Reaction I and II were mixed and kept under magnetic stirring for 24 h. The product was isolated by decanting and thoroughly washed with ethanol.

General procedure for Knoevenagel condensation using $\text{Fe}_3\text{O}_4 @ \text{SiO}_2$ -CPTMS-DABCO as catalyst

A mixture of the aldehyde/ketone (0.1 mmol), malononitrile (0.1 mmol), catalyst (10 mg) and solvent (ethanol, 0.4 mL) into a glass tube was mechanically stirred at 75 $^\circ\text{C}$. The progress of the reaction was



Scheme 1. Synthetic route of $\text{Fe}_3\text{O}_4@SiO_2\text{-CPTMS-DABCO}$.

monitored by thin layer chromatography (TLC). The catalyst was removed by magnetic separation, and the products were precipitated with the addition of ice water followed by filtration under reduced pressure or obtained by liquid-liquid extraction with ethyl acetate. All products were characterized by nuclear magnetic resonance ^{13}C and ^1H (NMR), and the spectra are in the Supplementary Information (SI) section.

General procedure for the synthesis of isatin- β -thiosemicarbazones using $\text{Fe}_3\text{O}_4@SiO_2\text{-CPTMS-DABCO}$ as catalyst

A mixture of isatin (0.2 mmol), 4-phenylthiosemicarbazide (0.2 mmol), catalyst (10 mg) and ethanol, (0.5 mL) into a glass tube was mechanically stirred at 75°C . The reaction was monitored by TLC. The catalyst was removed by magnetic separation, and the products were obtained by extraction with ethyl acetate. The compounds were purified by hot solubilization in DMSO followed by precipitation with ice water and filtration under reduced pressure. All products were characterized by nuclear magnetic resonance ^{13}C and ^1H (NMR) and the spectra are in the SI section.

General procedure of reuse of $\text{Fe}_3\text{O}_4@SiO_2\text{-CPTMS-DABCO}$ catalyst

Reuse tests of the catalyst were performed with the standard reaction after each run, the catalyst was separated by external magnet, recovered, washed with water and ethanol (both twice), and dried under vacuum to be reused in the next reaction cycles. The same procedure was performed five times more.

Results and Discussion

Characterization of the nanoparticles

FTIR spectrum for the Fe_3O_4 sample (Figure 1) is characterized by a strong band centered at 572 cm^{-1} , which can be attributed to the $\nu(\text{Fe-O})$ stretching of iron cations at tetrahedral and octahedral sites. The broad absorption band at 3394 cm^{-1} is assigned to the vibrational stretching mode of hydroxyl ions or water molecules coordinated to iron ions³⁰ or adsorbed on the matrix surface. It is noteworthy that FTIR spectrum for core-shell magnetic nanoparticles $\text{Fe}_3\text{O}_4@SiO_2$ (Figure 1) also presents the bands characteristic of the magnetite, indicating that the coating was only limited to the surface of the matrix. It was also possible to observe a band at 1070 cm^{-1} that may be assigned to the asymmetric stretching of the $\nu(\text{Si-O})$.

Figure 1 also shows the FTIR spectrum of the functionalized $\text{Fe}_3\text{O}_4@SiO_2\text{-CPTMS-DABCO}$ magnetic nanoparticles in the interval of $400\text{-}4000\text{ cm}^{-1}$. This spectrum exhibits two partially shrouded bands between 2800 and 3000 cm^{-1} that may be attributed to the C-H stretching of the $-\text{CH}_2$ group. In addition, it is possible to observe two other bands, one at 1216 cm^{-1} , referring to the C-N bond,³¹ and the second one at 1615 cm^{-1} that is characteristic of the C-N⁺ bond arising from the C-N bond between the chloride of CPTMS and DABCO.³² These results provide strong evidence of efficient processes of coating and functionalization of magnetic nanoparticles with SiO_2 and DABCO, respectively. Moreover, the elemental analysis results (C, H and N) of the $\text{Fe}_3\text{O}_4@SiO_2\text{-CPTMS-DABCO}$ catalyst, C: 14.70%, H: 3.21% and

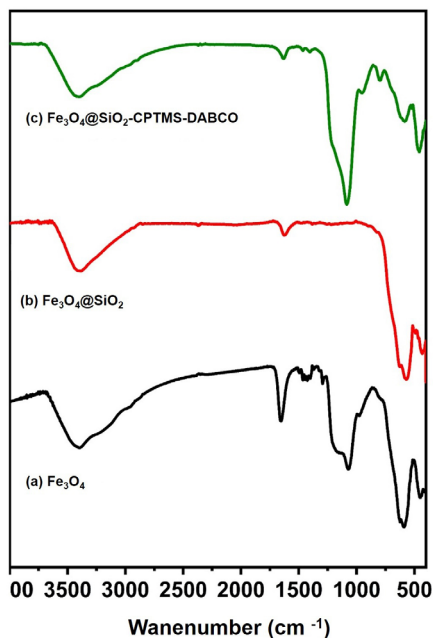


Figure 1. FTIR (KBr) spectra of the magnetic nanoparticles (a) Fe_3O_4 , (b) $\text{Fe}_3\text{O}_4@SiO_2$ and (c) $\text{Fe}_3\text{O}_4@SiO_2$ -CPTMS-DABCO.

N: 7.33% corroborate the FTIR data for efficient amine loading on the magnetic nanoparticle surface.

The powder X-ray diffraction (PXRD) data of the magnetic Fe_3O_4 , $\text{Fe}_3\text{O}_4@SiO_2$, $\text{Fe}_3\text{O}_4@SiO_2$ -CPTMS-DABCO nanoparticles are shown in Figure 2. The diffraction peaks and their relative intensities for all diffractograms are characteristic of magnetite (Fe_3O_4). These data are in agreement with the standard file (JCPDS No. 19-0629). For the $\text{Fe}_3\text{O}_4@SiO_2$ nanoparticle, a broad peak can also be observed in the range of $2\theta = 20$ - 30° due to the presence of amorphous siloxanes on the surface of the MNP. In the case of $\text{Fe}_3\text{O}_4@SiO_2$ -CPTMS-DABCO nanoparticles, this peak appears with a higher intensity referencing the development of the siloxane network on its surface.

As shown in the SEM images (Figures 3a, 3b and 3c), no significant changes in the morphological characteristics of the magnetite sample can be seen after the SiO_2 coating and functionalization process. The nanoparticles present

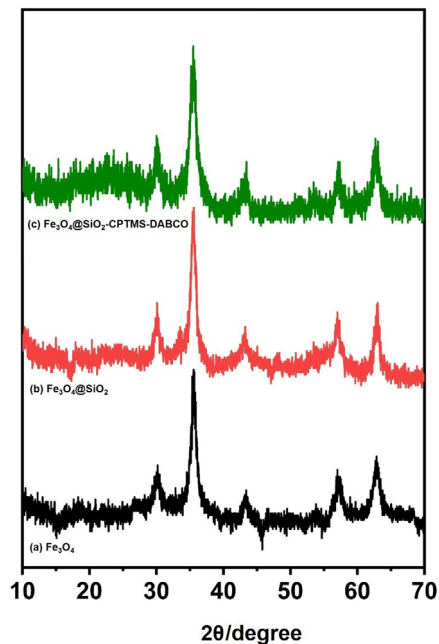


Figure 2. Powder X-ray (PXRD) diffractograms of the (a) Fe_3O_4 , (b) $\text{Fe}_3\text{O}_4@SiO_2$ and (c) $\text{Fe}_3\text{O}_4@SiO_2$ -CPTMS-DABCO.

the same granular structure consisting of submicrometer particles. In the images provided by TEM, it is observed that the $\text{Fe}_3\text{O}_4@SiO_2$ particles (Figure 3b) present lower contrast contours, indicating the coating effectuation. According to the TEM images, the size of magnetite particles is between 150 and 250 nm, being formed with aggregates smaller than 20 nm, as described in the literature.³³ The SEM analyses of the $\text{Fe}_3\text{O}_4@SiO_2$ -CPTMS-DABCO catalyst corroborate the data reported by Gupta *et al.*³⁴

Figure 4 shows the thermal stability analysis data for the Fe_3O_4 , $\text{Fe}_3\text{O}_4@SiO_2$ and $\text{Fe}_3\text{O}_4@SiO_2$ -CPTMS-DABCO materials. Overall, the first weight loss event in the 25-300 °C interval may be assigned to water or solvent molecules adsorbed on the surface of the materials or trapped in their structures. Thermogravimetric analysis (TGA) curve for the $\text{Fe}_3\text{O}_4@SiO_2$ -CPTMS-DABCO nanoparticles (Figure 4) had suffered the first mass loss at 120 °C, which is also related to solvent molecules (water or ethanol). In the range from 300 to 650 °C, a weight loss of

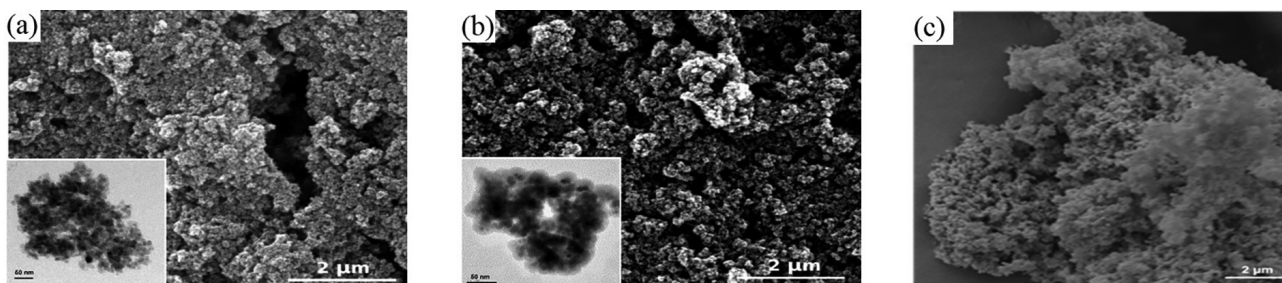


Figure 3. Representative images obtained by SEM (larger image) and TEM (smaller image) for the materials: (a) Fe_3O_4 , (b) $\text{Fe}_3\text{O}_4@SiO_2$ and (c) $\text{Fe}_3\text{O}_4@SiO_2$ -CPTMS-DABCO.

about 55% is observed, which is related to functionalization with CPTMS-DABCO.

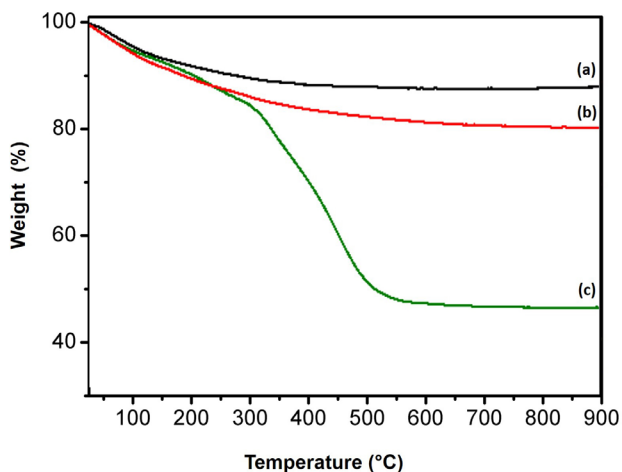


Figure 4. TGA curves of the (a) Fe_3O_4 , (b) $\text{Fe}_3\text{O}_4@SiO_2$ and (c) $\text{Fe}_3\text{O}_4@SiO_2$ -CPTMS-DABCO MNPs.

Figure 5 depicts the quantum design vibrating sample magnetometer (VSM) data of the materials measured at room temperature under an applied field range from -10000 to 10000 Oe. The magnetic measurements showed nearly zero values of coercivity (H_c) and remaining magnetization (σ_r), suggesting that the materials exhibit superparamagnetic behavior.³⁵⁻³⁷ The saturation magnetization (M_s) values of the materials decrease significantly from Fe_3O_4 nanoparticles ($M_s = 61.01 \pm 0.01 \text{ emu g}^{-1}$) to the covered $\text{Fe}_3\text{O}_4@SiO_2$ ($M_s = 38.60 \pm 0.01 \text{ emu g}^{-1}$) and functionalized $\text{Fe}_3\text{O}_4@SiO_2$ -CPTMS-DABCO ($M_s = 23.5 \pm 0.01 \text{ emu g}^{-1}$) materials. This behavior reflects the successful coating and functionalization processes of the particles, providing

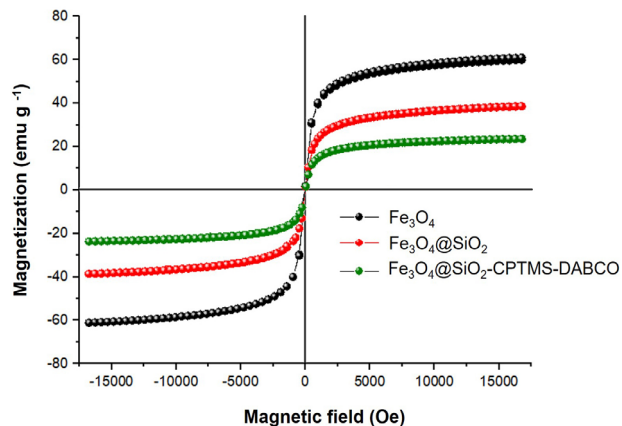


Figure 5. Hysteresis curves for magnetic nanoparticles Fe_3O_4 , $\text{Fe}_3\text{O}_4@SiO_2$ and $\text{Fe}_3\text{O}_4@SiO_2$ -CPTMS-DABCO.

a lower value of magnetite *per gram*. However, the $\text{Fe}_3\text{O}_4@SiO_2$ -CPTMS-DABCO catalyst retained sufficient magnetization to allow magnetic separation by an external magnet.

Catalytic activity

Application of $\text{Fe}_3\text{O}_4@SiO_2$ -CPTMS-DABCO in Knoevenagel condensation

The first trials were performed employing the $\text{Fe}_3\text{O}_4@SiO_2$ -CPTMS-DABCO catalyst in the reaction between malononitrile and benzaldehyde with varying amounts of catalyst, solvents and temperature (Table 1). The Knoevenagel condensation without catalyst (Table 1, entry 1) took place in 60 min and gave excellent yield. Interestingly, a short time was found for reactions carried out using $\text{Fe}_3\text{O}_4@SiO_2$ -CPTMS-DABCO as catalyst

Table 1. $\text{Fe}_3\text{O}_4@SiO_2$ -CPTMS-DABCO-catalyzed Knoevenagel condensation between benzaldehyde and malononitrile under different conditions

entry	Catalyst	Mass / mg	Solvent	time / min	Isolated yield / %
1	–	–	EtOH	60	92
2	$\text{Fe}_3\text{O}_4@SiO_2$ -CPTMS-DABCO	10	EtOH	15	99
3	$\text{Fe}_3\text{O}_4@SiO_2$ -CPTMS-DABCO	5	EtOH	20	95
4	$\text{Fe}_3\text{O}_4@SiO_2$ -CPTMS-DABCO	15	EtOH	15	99
5	$\text{Fe}_3\text{O}_4@SiO_2$ -CPTMS-DABCO	10	EtOH	120	93 ^a
6	$\text{Fe}_3\text{O}_4@SiO_2$ -CPTMS-DABCO	10	H_2O	25	88
7	$\text{Fe}_3\text{O}_4@SiO_2$ -CPTMS-DABCO	10	toluene	30	91
8	$\text{Fe}_3\text{O}_4@SiO_2$	10	EtOH	60	trace
9	DABCO	10	EtOH	30	89
10	–	–	EtOH	15	39

^aRoom temperature. Reaction conditions: benzaldehyde (0.1 mmol), malononitrile (0.1 mmol), solvent (0.4 mL). CPTMS: 3-chloropropyltrimethoxysilane; DABCO: 1,4-diazabicyclo[2,2,2]octane.

(entry 2). The best result for the Knoevenagel **1a** product, varying the catalyst load (Table 1, entry 2, 3 and 4) was observed using 10 mg of $\text{Fe}_3\text{O}_4@\text{SiO}_2\text{-CPTMS-DABCO}$, in ethanol as solvent under reflux (Table 1, entry 2), promoting the reaction in just 15 min with 99% isolated yield.

The use of toluene (Table 1, entry 7) as a more apolar solvent and water (Table 1, entry 6) as a more polar solvent led to lower isolated yields of Knoevenagel compounds with lower yields (91 and 88%) and longer times (30 and 25 min), respectively. When the reaction was tested at room temperature (Table 1, entry 5), the reaction time was 120 min, demonstrating that temperature plays an important role on the reaction kinetics. The reaction with the $\text{Fe}_3\text{O}_4@\text{SiO}_2$ matrix (Table 1, entry 8) generated only traces of product (60 min), suggesting that the silanol groups on the silica surface act as inefficient acid sites for reaction catalysis, corroborating studies by Resende Filho *et al.*³⁸ and Chen *et al.*³⁹ The use of only DABCO as catalyst (Table 1, entry 9) also produces compound **1a** although with a longer reaction time and lower yield.

In Scheme 2, a mechanism is proposed for the reaction between benzaldehyde and malononitrile using the catalyst $\text{Fe}_3\text{O}_4@\text{SiO}_2\text{-CPTMS-DABCO}$ based on the proposal by Meng *et al.*⁴⁰ The first stage consists of the deprotonation of active methylene by the catalyst. Then, the carbanion attacks the carbonyl of the aldehyde to form the enolate, and this is then protonated by the catalyst, generating alcohol (stage 2). In stage 3, the catalyst promotes α -deprotonation of alcohol, giving rise to the formation of a C=C double

bond, which ends up inducing the removal of the hydroxyl group by elimination E1cB, which leads to the formation of the final product (**1a**). The hydroxyl in the middle will be protonated, forming H_2O and restoring the catalyst (stage 4).

The $\text{Fe}_3\text{O}_4@\text{SiO}_2\text{-CPTMS-DABCO}$ catalyst under the optimized conditions was applied in Knoevenagel reactions with substituted benzaldehydes to evaluate the influence of steric and electronic factors, as well as other aromatic and aliphatic aldehydes (Figure 6).

In general, all reactions in Figure 6 showed good isolated yields (84-99%) and considerably short

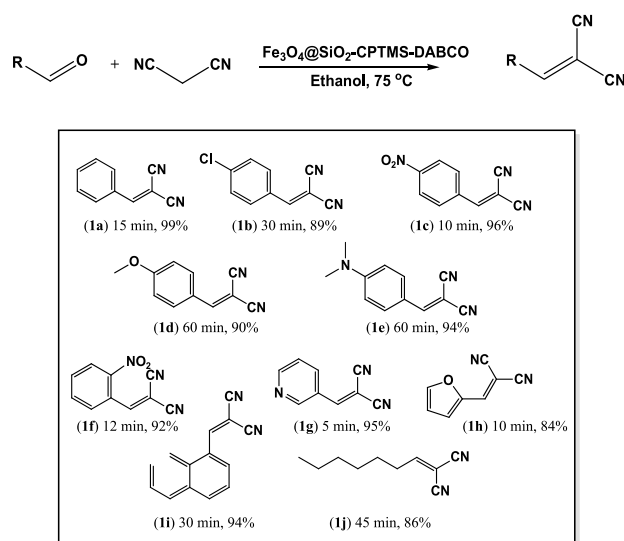
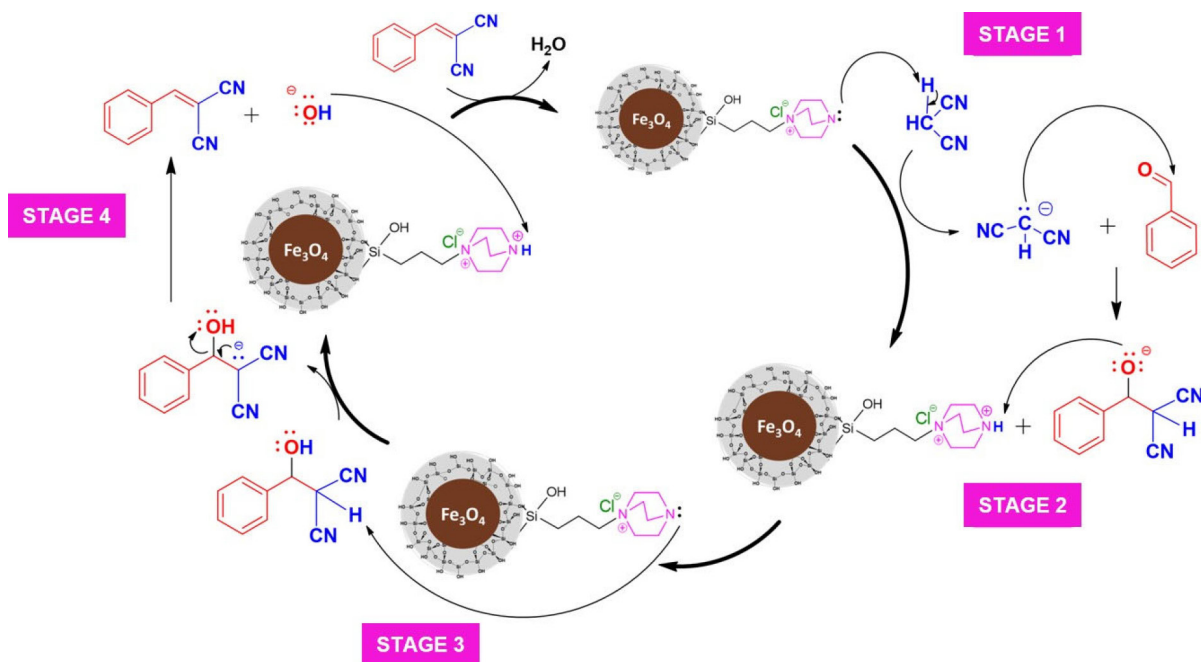


Figure 6. Knoevenagel condensation of substituted aldehydes with malononitrile in the presence of $\text{Fe}_3\text{O}_4@\text{SiO}_2\text{-CPTMS-DABCO}$.



Scheme 2. Proposed mechanism of action of the catalyst $\text{Fe}_3\text{O}_4@\text{SiO}_2\text{-CPTMS-DABCO}$ in the Knoevenagel condensation reaction.

reaction times (from 5-60 min), primarily when related to other catalysts supported on MNPs reported in the literature.^{24,41,42} The reaction with the chloro substituent at position 4 (**1b**) presented a longer reaction time and lower yield than the reaction with unsubstituted benzaldehyde (**1a**), which is in agreement to the previous work reported by Abrantes *et al.*¹⁹ Nitro substituted benzaldehydes (**1c**) and (**1f**) showed the shortest reaction times among all monosubstituted benzaldehydes tested. However, in the reaction with 2-NO₂-benzaldehyde (**1f**), a slightly longer reaction time was observed, probably due to the steric hindrance from the substituent group in the *ortho* position.

The reactions with electron donor groups at position 4 (**1d** and **1e**) were synthesized in longer times (60 min) due to the deactivation of the aldehyde carbonyl. In the studies by Kakesh *et al.*,⁴³ a MNP coated with poly(ionic liquid) (Fe₃O₄-PIL) was investigated in the Knoevenagel reaction in an aqueous medium and using ultrasound irradiation. Although products **1d** and **1e** were also obtained in the same reaction time (60 min), their isolated yields were lower than those reported in this work.

The products from heteroaromatic aldehydes (**1g** and **1h**) showed shorter reaction times compared to benzaldehyde (**1a**), suggesting that the inductive effect of the heteroatom favors the electrophilicity of the carbonyl. The substrate 3-pyridinecarboxyaldehyde (**1g**) is a very reactive electrophile, showed the shortest reaction time of the studied aldehydes (5 min), with 95% yield. The reaction time of the substrate 2-naphthalaldehyde (**1i**) was slower compared to the other aromatic aldehydes, probably due to the steric hindrance. Reactions with the aliphatic aldehyde heptanal (**1j**) were also investigated, showing similar reactivity to the aromatics considering the reaction time.

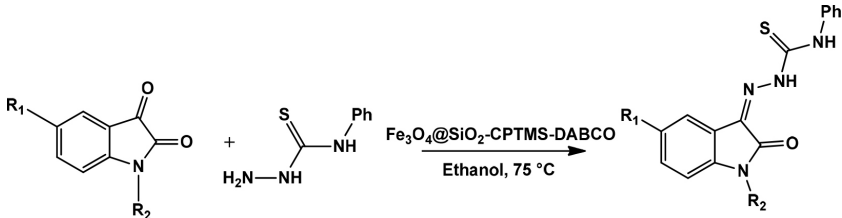
Application of Fe₃O₄@SiO₂-CPTMS-DABCO in the synthesis of isatin-β-thiosemicarbazones

The Fe₃O₄@SiO₂-CPTMS-DABCO catalyst was also applied to the reaction between isatin and 4-phenylthiosemicarbazide to evaluate its ability to obtain isatin-β-thiosemicarbazones (**2a**) or its spiro derived⁴⁴ from the nucleophilic addition of semicarbazide to isatin. The methodology employed in the initial tests of this reaction was based on the study by Seifi and Sheibani,⁴⁵ in which equivalent amounts of isatin, semicarbazides, and triethylamine (0.2 mL) in absolute ethanol (20 mL) were stirred for 5 h at reflux. However, in our methodology, 10 mg of catalyst was used and after 60 min, only compound (**2a**) was obtained with 94% isolated yield (Table 2). The same reaction performed without catalyst occurred in 90 min with 90% yield.

The Fe₃O₄@SiO₂-CPTMS-DABCO was employed in the investigation of the reaction of other substituted isatins with 4-phenylthiosemicarbazide (Table 2).

The data presented in Table 2 shows that the synthesis of isatin-β-thiosemicarbazones (**2a-2d**) employing the catalyst Fe₃O₄@SiO₂-CPTMS-DABCO resulted in shorter reaction times and yields very close to or higher than those described in the literature.^{44,46} It is worth mentioning that generally, these reactions are carried out at reflux, lasting between 2-5 h.^{44,46} It can be observed that for thiosemicarbazone without substituent (**2a**), the reaction time was shorter than the other products obtained and with a yield of 94% in just 60 min. The chlorinated (**2c**) and *N*-methylated (**2d**) thiosemicarbazones were synthesized with very close yields. However, the reaction time for the product (**2d**) was almost double that for compound **2c**, indicating that the presence of the methyl altered the reactivity of the isatin derivative.

Table 2. The synthesis of isatin-β-thiosemicarbazones catalyzed by Fe₃O₄@SiO₂-CPTMS-DABCO



entry	Compound	R ₁	R ₂	time / min	Isolated yield / %
1	2a	H	H	60	94
2	2b	Br	H	180	81
3	2c	Cl	H	80	94
4	2d	H	CH ₃	150	93

Reaction conditions: isatin (0.1 mmol), thiosemicarbazide (0.1 mmol), catalyst (10 mg), solvent (0.5 mL).

Brominated thiosemicarbazone (**2b**) was obtained with lower yield, suggesting that the presence of halogen may be reducing the electrophilicity of the C-3 carbon, making the direct condensation of isatin and thiosemicarbazide difficult. In studies developed by Somogyi *et al.*,⁴⁶ thiosemicarbazones were synthesized, including the product (**2d**). For this, equimolar conditions of isatin and thiosemicarbazide, with acetic acid as a catalyst, were used under heating. However, despite presenting a 4% higher yield, compound **2d** was obtained after 4 h of reaction, while in this work, it took 2.5 h. In work reported by Zhang and co-workers,⁴⁴ equimolar ratios of isatin and thiosemicarbazones were also used. Nonetheless, in addition to acetic acid (as a catalyst), the authors used EtOH as solvent to obtain the products (**2a**) and (**2b**).

Reuse of $\text{Fe}_3\text{O}_4@SiO_2\text{-CPTMS-DABCO}$ in Knoevenagel reaction and synthesis of isatin- β -thiosemicarbazones

After each run, the $\text{Fe}_3\text{O}_4@SiO_2\text{-CPTMS-DABCO}$ catalyst was separated by an external magnetic magnet (Figure 7), recovered, washed with water and ethanol (both twice), and dried under reduced pressure to be reused in the successive reaction cycles. Interestingly, the $\text{Fe}_3\text{O}_4@SiO_2\text{-CPTMS-DABCO}$ catalyst proved to be robust and efficient under the conditions employed with no considerable reduction in catalytic activity until the fifth reuse cycle (Figure 8). FTIR spectra of the novel catalyst with the reused catalyst are quite similar, indicating that no chemical changes in the catalyst structure with the number of cycles that could impair its catalytic activity has occurred (up to six times Figure 9).

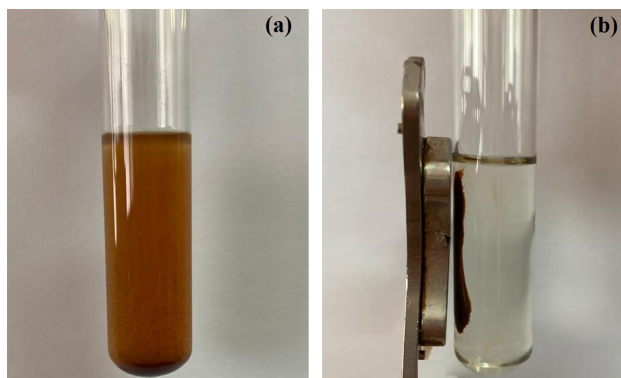


Figure 7. Reuse of the $\text{Fe}_3\text{O}_4@SiO_2\text{-CPTMS-DABCO}$ catalyst: (a) dispersed in the reaction medium and (b) facing the magnetic response stimulated by an external magnet.

Conclusions

In conclusion, a methodology for synthesizing a catalyst based on Fe_3O_4 MNPs previously coated with SiO_2 and

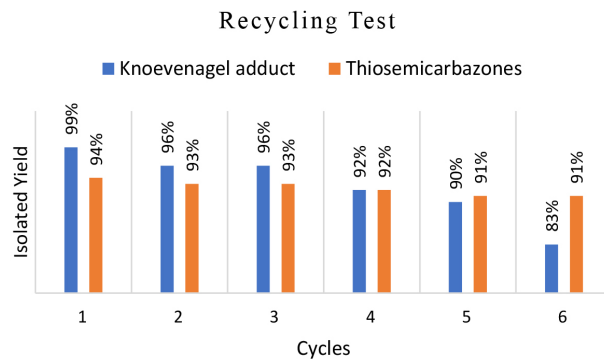


Figure 8. Reuse of $\text{Fe}_3\text{O}_4@SiO_2\text{-CPTMS-DABCO}$ catalyst in synthesis of Knoevenagel compound (**1a**) and isatin- β -thiosemicarbazone (**2a**).

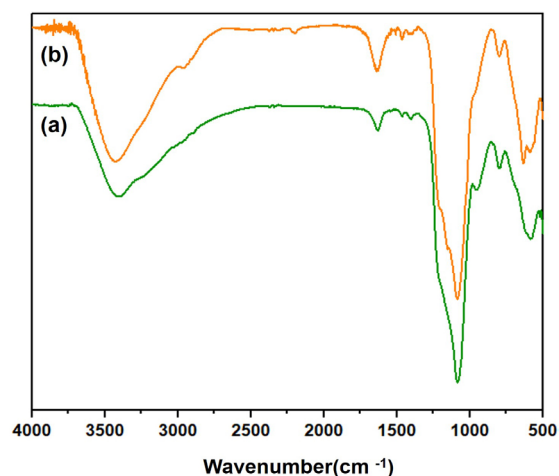


Figure 9. FTIR (KBr) spectra of the (a) the $\text{Fe}_3\text{O}_4@SiO_2\text{-CPTMS-DABCO}$ nanoparticles and (b) the reused (6-fold) $\text{Fe}_3\text{O}_4@SiO_2\text{-CPTMS-DABCO}$ catalyst, recorded in the spectral range of 400-4000 cm^{-1} .

sequentially functionalized with DABCO is proposed. Overall, the nanocatalyst showed remarkable performance and excellent catalytic activity even at low concentrations and mild conditions, with isolated yields between 84-99% and reaction times between 5-60 min for the Knoevenagel reaction. For the synthesis of isatin- β -thiosemicarbazone the formation of products with isolated yields between 81-94% and reaction times of 60-180 min was observed. The catalyst was easily recovered under an external magnetic field and reused for 6 cycles without significant loss of its catalytic activity.

Supplementary Information

Supplementary information (materials, apparatus and characterizations details) is available free of charge at <http://jbcbs.sbq.org.br> as PDF file.

Acknowledgments

This work is funded by the Conselho Nacional de

Desenvolvimento Científico and Tecnológico (CNPQ) and Coordenação de Aperfeiçoamento de Pessoal de Nível Superior (CAPES). The authors also thanks Unical (Unit of the Analytical Center) and IPeFarM-UFPB (Institute of Research in Drugs and Medicines of UFPB) for assistance in the NMR analysis.

Author Contributions

Nathalia Kellyne S. M. Falcão was responsible for investigation, methodology, data curation, validation, writing-review and editing; Gilvan P. Pires for investigation, methodology, data curation, validation, writing-review and editing; Paloma G. Abrantes for data curation, formal analysis, investigation, methodology; Poliana G. Abrantes for data curation, formal analysis, investigation, methodology; João B. M. Resende Filho for data curation, formal analysis, investigation, methodology; Cláudio G. Lima Júnior for data curation, formal analysis, investigation, investigation, methodology; Ercules E. S. Teotonio for data curation, formal analysis, investigation, investigation, methodology; Juliana A. Vale for data curation, formal analysis, methodology, funding acquisition, project administration, investigation, methodology, supervision.

References

- Shiri, L.; Ghorbani-Choghamarani, A.; Kazemi, M.; *Aust. J. Chem.* **2017**, *32*, 9. [Crossref]
- Shiri, L.; Narimani, H.; Kazemi, M.; *Appl. Organomet. Chem.* **2018**, *32*, e3927. [Crossref]
- Shiri, L.; Zarei, S.; Kazemi, M.; Sheikh, D.; *Appl. Organomet. Chem.* **2018**, *32*, e3938. [Crossref]
- Shiri, L.; Kazemi, M.; Heidari, L.; *Appl. Organomet. Chem.* **2018**, *32*, e3943. [Crossref]
- Senapati, K. K.; Roy, S.; Borgohain, C.; Phukan, P.; *J. Mol. Catal. A: Chem.* **2012**, *352*, 128. [Crossref]
- Shao, H.; Yoon, T. J.; Liang, M.; Weissleder, R.; Lee, H.; *Beilstein J. Nanotechnol.* **2010**, *1*, 142. [Crossref]
- Colombo, M.; Carregal-Romero, S.; Casula, M. F.; Gutierrez, L.; Morales, M. P.; Boehm, I. B.; Hever-Hagen, J. T.; Prospero, D.; Parak, W. J.; *Chem. Soc. Rev.* **2012**, *41*, 4306. [Crossref]
- Chen, M.-N.; Mo, L.-P.; Cui, Z.-S.; Zhang, Z.-H.; *Curr. Opin. Green Sustainable Chem.* **2019**, *15*, 27. [Crossref]
- Kim, D. K.; Mikhaylova, M.; Wang, F. H.; Kehr, J.; Bjelke, B.; Zhang, Y.; Tsakalagos, T.; Muhammed, M.; *Chem. Mater.* **2003**, *15*, 4343. [Crossref]
- Chaturvedi, S.; Dave, P. N.; Shah, N. K.; *J. Saudi Chem. Soc.* **2012**, *16*, 307. [Crossref]
- Karimi, B.; Mansouri, F.; Mirzaei, H. M.; *ChemCatChem* **2015**, *7*, 1736. [Crossref]
- Salgueiriño-Maceira, V.; Correa-Duarte, M. A.; *Adv. Mater.* **2007**, *19*, 4131. [Crossref]
- Yeap, S. P.; Lim, J.; Ooi, B. S.; Ahmad, A. L.; *J. Nanopart. Res.* **2017**, *19*, 368. [Crossref]
- Schärtl, W.; *Nanoscale* **2010**, *2*, 829. [Crossref]
- Wang, D.; Deraedt, C.; Salmon, L.; Labrugere, C.; Etienne, L.; Ruiz, J.; Astruc, D.; *Chem. Eur. J.* **2015**, *21*, 1508. [Crossref]
- Zanin, L. L.; Jimenez, D. E. Q.; Fonseca, L. P.; Porto, A. L. M.; *Curr. Org. Chem.* **2018**, *22*, 519. [Crossref]
- Vaid, R.; Gupta, M.; *Monatsh Chem.* **2015**, *146*, 645. [Crossref]
- Zhang, Y.; Xia, C.; *Appl. Catal., A* **2009**, *366*, 141. [Crossref]
- de Abrantes, P. G.; Costa, I. F.; Falcão, N. K. S. M.; Ferreira, J. M. G. O.; Lima Jr., C. G.; Teotonio, E. E. S.; Vale, J. A.; *Catal. Lett.* **2022**, 152. [Crossref]
- Chen, H.; Fan, L.; Zhang, X.; *ACS Appl. Mater. Interfaces* **2020**, *12*, 54884. [Crossref]
- Xu, B.; Liu, Z.; Xu, Q.; Han, X.; Ma, X.; Wang, J.; Kannan, T.; Ma, P.; Wang, J.; Niu, J.; *J. Mater. Sci.* **2021**, *56*, 4654. [Crossref]
- Zengin, N.; Burhan, H.; Şavk, A.; Göksu, H.; Şen, F.; *Sci. Rep.* **2020**, *10*, 12758. [Crossref]
- Balachandran, C.; Haribabu, J.; Jeyalakshmi, K.; Bhuvanesh, N. S. P.; Karvembu, R.; Emi, N.; Awale, S.; *J. Inorg. Biochem.* **2018**, *182*, 208. [Crossref]
- Pervez, H.; Iqbal, M. S.; Tahir, M. Y.; Choudhary, M. I.; Khan, K. M.; *Nat. Prod. Res.* **2007**, *21*, 1178. [Crossref]
- Cunha, S.; Silva, T. L.; *Tetrahedron Lett.* **2009**, *50*, 2090. [Crossref]
- Ali, A. Q.; Teoh, S. G.; Salhin, A.; Eltayeb, N. E.; Khadeer, A. M. B.; Majid, A. M. S. A.; *Spectrochim. Acta, Part A* **2014**, *125*, 440. [Crossref]
- Kang, I. J.; Wang, L. W.; Hsu, T. A.; Yueh, A.; Lee, C. C.; Lee, Y. C.; Chao, Y. R.; Shih, S. R.; Chern, J. H.; *Bioorg. Med. Chem. Lett.* **2011**, *21*, 1948. [Crossref]
- Arenas, L. T.; Aguirre, T. A. S.; Langaro, A.; Gushikem, Y.; Benvenutti, E. V.; Costa, T. M. H.; *Polymer* **2003**, *44*, 5521. [Crossref]
- Arenas, L. T.; Lima, E. C.; dos Santos Jr., A. A.; Vaghetto, J. C. P.; Costa, T. M. H.; Benvenutti, E. V.; *Colloids Surf., A* **2007**, *297*, 240. [Crossref]
- Kainz, Q. M.; Reiser, O.; *Acc. Chem. Res.* **2014**, *47*, 667. [Crossref]
- Yang, F.; Wang, Z.; Wang, H.; Wang, C.; Wang, L.; *RSC Adv.* **2015**, *5*, 57122. [Crossref]
- Hasaninejad, A.; Shekouhy, M.; Golzar, N.; Zare, A.; Doroodmand, M. M.; *Appl. Catal., A* **2011**, *402*, 11. [Crossref]
- Rostami, A.; Atashkar, B.; Gholami, H.; *Catal. Commun.* **2013**, *37*, 69. [Crossref]
- Gupta, R.; Yadav, M.; Gaur, R.; Arora, G.; Rana, P.; Yadav, P.; Adholeya, A.; Sharma, R. K.; *ACS Omega* **2019**, *4*, 21529. [Crossref]
- Pan, X.; Guan, J.; Yoo, J. W.; Epstein, A. J.; Lee, L. J.; Lee, R. J.; *Int. J. Pharm.* **2008**, *358*, 263. [Crossref]

36. Rahman, O.; Mohapatra, S. C.; Ahmad, S.; *Mater. Chem. Phys.* **2012**, *132*, 196. [Crossref]
37. Yin, S.; Sun, J.; Liua, B.; Zhang, Z.; *J. Mater. Chem. A* **2015**, *3*, 4992. [Crossref]
38. de Resende Filho, J. B. M.; Pires, G. P.; Ferreira, J. M. G. O.; Teotonio, E. E. S.; Vale, J. A.; *Catal. Lett.* **2017**, *147*, 167. [Crossref]
39. Chen, X.; Arruebo, M.; Yeung, K. L.; *Catal. Today* **2013**, *204*, 140. [Crossref]
40. Meng, D.; Qiao, Y.; Wang, X.; Wen, W.; Zhao, S.; *RSC Adv.* **2018**, *8*, 30180. [Crossref]
41. Kumar, A.; Dewan, M.; Saxena, A.; De, A.; Mozumdar, S.; *Catal. Commun.* **2010**, *11*, 679. [Crossref]
42. Fang, Y.; Wang, X.; Chen, Y.; Dai, L.; *J. Zhejiang Univ., Sci., A* **2020**, *21*, 74. [Crossref]
43. Kakesh, N.; Sayyahi, S.; Badri, R.; *C. R. Chim.* **2018**, *21*, 1023. [Crossref]
44. Zhang, X.-M.; Guo, H.; Li, Z. S.; Song, F. H.; Wang, W. M.; Dai, H.-Q.; Zhang, L.-X.; Wang, J.-G.; *Eur. J. Med. Chem.* **2015**, *101*, 419. [Crossref]
45. Seifi, M.; Sheibani, H.; *Lett. Org. Chem.* **2013**, *10*, 478. [Crossref]
46. Somogyi, L.; *Liebigs Ann. Chem.* **1993**, *8*, 931. [Crossref]

Submitted: November 14, 2022

Published online: March 7, 2023

